

ENHANCED DETECTION OF TINY OBJECTS IN AERIAL IMAGES

Kihyun Kim^{*1} Michalis Lazarou² Tania Stathaki¹
yoo07220@gmail.com michalislazarou93@gmail.com t.stathaki@imperial.ac.uk

¹ Dept of Electrical & Electronic Engineering, Imperial College London

² Center for Vision, Speech and Signal Processing, University of Surrey

Abstract—While one-stage detectors like YOLOv8 offer fast training speed, they often under-perform on detecting small objects as a trade-off. This becomes even more critical when detecting tiny objects in aerial imagery due to low-resolution targets and cluttered backgrounds. To address this, we introduce three enhancement strategies—*input image resolution adjustment, data-augmentation and attention mechanism*—that can be easily implemented on YOLOv8. We demonstrate that image size enlargement and the proper use of augmentation can lead to enhancement. Additionally, we designed a **Mixture of Orthogonal Neural-modules Network(MoonNet)** pipeline which consists of attention-augmented CNNs. Two well-known attention modules Squeeze-and-Excitation Block (SE Block) and Convolutional Block Attention Modules (CBAM) were integrated to the backbone of YOLOv8 with the increased number of channels and the MoonNet backbone obtained improved detection accuracy compared to that of the original YOLOv8. MoonNet further proved its adaptability and potential by achieving state-of-the-art performance on tiny object benchmark when integrated with the YOLC model. Our codes are available at:<https://github.com/Kihyun11/MoonNet>

Index Terms— Tiny object detection, Deep learning, Attention mechanism, YOLO

1. INTRODUCTION

Advances in deep learning have transformed object detection, evolving from early sliding-window CNNs such as R-CNN [1] to modern pyramidal, end-to-end architectures. Two-stage detectors—including Faster R-CNN [2], Feature Pyramid Networks (FPN) [3], and Mask R-CNN [4]—first generate region proposals and then refine classification and localization, achieving state-of-the-art accuracy. In parallel, one-stage models prioritise speed by eliminating the proposal stage; seminal examples include SSD [5] and the “You Only Look Once” (YOLO)

family [6] [7]. Although one-stage detectors excel in training speed, they tend to struggle with detecting tiny objects as a design trade-off. This limitation is especially pronounced in aerial imagery, where targets often occupy only a few pixels amid cluttered backgrounds. This work addresses the challenge of tiny-object detection, using YOLOv8. Our contributions are threefold: (i) higher input resolution, (ii) targeted data augmentation, and (iii) an attention-augmented backbone—each yielding measurable gains.

2. RELATED WORK

Previous studies using YOLO: Plenty of researches specifically targeting the enhancement of tiny object detection using the YOLO model already exists. Ma et al. [8] improve YOLOv8s for tiny-object detection by substituting standard strided convolutions with the SPD-Conv module and replacing the PANet neck with SPANet, achieving finer feature preservation and stronger multi-scale fusion. Hu et al. [9] enhance YOLOv5 through an Efficient Spatial Pyramid Pooling (ESPP) module, raising small-object accuracy in aerial imagery while keeping the network lightweight.

Tiny object detection in general: Prior work has explored various methods for tiny object detection. Xu et al. [10] suggests that effective enhancement methods for tiny object detection can be categorized into five: *multi-scale feature learning, context based detection, data augmentation, designing better training strategy and label assignment strategy*. High resolution imagery is crucial as well and numerous approaches were made to improve the resolution of the images such as Query-Det [11]. Some studies such as YOLC [12] even use cropping-method to make the training more efficient.

Input image resolution: Yan et al. [13] demonstrated that increasing the input image resolution can significantly improve the detection of small-scale objects, as it enables the model to capture more detailed features. Motivated by this, we experiment with multiple input image resolutions in this study to assess their impact.

^{*}Thanks to Hyeosoon Kim and Seonhwan Kim for funding & support

Data Augmentation: Proper augmentation is critical when dealing with limited and highly imbalanced datasets. Kisantal et al. [14] identified the scarcity of images containing tiny objects and their limited representation in the dataset as a major challenge for small object detection. They addressed this issue using a copy-paste augmentation strategy.

Attention Mechanism: Hu et al. [15] proposed the Squeeze-and-Excitation (SE) block to enhance CNNs by modeling inter-channel dependencies and recalibrating feature responses. Woo et al. [16] extended this with the Convolutional Block Attention Module (CBAM), which combines channel and spatial attention to better focus on informative regions—an advantage in tiny object detection where spatial precision is crucial.

3. METHODOLOGY

3.1. Enhancement Strategy

In total, three different enhancement strategies were implemented on the YOLOv8 to obtain efficient training.

Varying the input image resolution: Three different input image resolutions 640, 800 and 928 were tested.

Data Augmentation: A diverse set of data augmentation techniques was applied. These included geometric transformations (rotations, horizontal and vertical flips), photometric adjustments (brightness and contrast variation), and random noise injection. While these augmentations simulated real-world variations, the primary motivation was to mitigate class imbalance—particularly for under-represented tiny object categories.

Attention Modules Integration: To improve the model’s sensitivity to fine-grained details, attention mechanisms were integrated into the YOLOv8 backbone. Specifically, Squeeze-and-Excitation (SE) blocks and Convolutional Block Attention Modules (CBAM) were inserted directly into select convolutional layers of the backbone. Instead of implementing them as standalone modules, the convolution layer class was extended to perform channel-wise recalibration (SE) and spatial attention (CBAM) inline. This design minimized architectural complexity and computational overhead while enhancing the model’s focus on salient regions critical for tiny object detection.

3.2. Final Configuration

Following a multi-stage optimization process, the final model configuration was determined by selecting the most effective combinations of image resolution, data augmentation techniques, and network architecture. Using the modified backbone with integrated attention modules and the best-performing input image resolution setting, the final model was trained from scratch.

3.3. Integration with YOLC

The attention modules are also integrated to the backbone of the YOLC[12] with the following modifications:

Squeeze-Excitation Operation (Ours)

$$x \in \mathbb{R}^{C \times H \times W}, \quad (1a)$$

$$c = \text{GlobalAvgPool}(x) \in \mathbb{R}^{C \times 1 \times 1}, \quad (1b)$$

$$z = W_2 \phi(W_1 c), \quad \phi = \text{ReLU}, \quad (1c)$$

$$y_{\text{original}} = x \odot \sigma(z), \quad \sigma = \text{sigmoid}, \quad (1d)$$

$$y_{\text{ours}} = x \odot (1 + \tanh(z)). \quad (1e)$$

CBAM Operation (Ours)

$$x \in \mathbb{R}^{C \times H \times W}, \quad (2a)$$

$$c_{\text{avg}} = \text{GlobalAvgPool}(x), \quad (2b)$$

$$c_{\text{max}} = \text{GlobalMaxPool}(x), \quad (2c)$$

$$z_c = W_2 \phi(W_1 c_{\text{avg}}) + W_2 \phi(W_1 c_{\text{max}}), \quad (2d)$$

$$x_c^{\text{original}} = x \odot \sigma(z_c), \quad (2e)$$

$$x_c^{\text{ours}} = x \odot (1 + \tanh(z_c)), \quad (2f)$$

$$f_{\text{avg}} = \text{Avg}_{\text{chan}}(x_c^{\bullet}), \quad f_{\text{max}} = \text{Max}_{\text{chan}}(x_c^{\bullet}), \quad (2g)$$

$$z_s = \text{Conv}_{k \times k}([f_{\text{avg}}, f_{\text{max}}]), \quad (2h)$$

$$y_{\text{original}} = x_c^{\text{original}} \odot \sigma(z_s), \quad (2i)$$

$$y_{\text{ours}} = x_c^{\text{ours}} \odot (1 + \tanh(z_s)). \quad (2j)$$

Parameters & notes: $W_1 \in \mathbb{R}^{m \times C}$, $W_2 \in \mathbb{R}^{C \times m}$, $m = \max(8, \lfloor C/r \rfloor)$ for reduction ratio $r > 0$. Channel logits z (SE) and z_c (CBAM) lie in \mathbb{R}^C and are broadcast over $H \times W$ (equivalently reshape to $C \times 1 \times 1$). Spatial logits $z_s \in \mathbb{R}^{1 \times H \times W}$ are broadcast over channels. Here \odot denotes element-wise multiplication, and x_c^{\bullet} denotes the branch (original/ours) passed to the spatial gate. x denotes the input feature map and the subscript *chan* means channel-wise. All the variables with ‘original’ subscript denotes the original operation whereas that with ‘ours’ denotes the modified operation.

Motivation. In preliminary trials, with the attention-attached HRNet backbone, the YOLC model learned nothing. We claimed the major cause of this result as a sigmoid gating which halves the output signal right away. Our modification replaces the sigmoid gate with a *residual, zero-centered* gate $x \odot (1 + \tanh(\cdot))$ and uses identity-safe init (set the last projection(s) to zero) so $z=0 \Rightarrow y_{\text{ours}}=x$ at step 0.

Placement. Attention is applied *per branch at the outputs of the final HRNet stage* (post-branch adapters), not inside internal convolutional blocks. Let $\{f^{(i)}\}_{i=1}^B$ be the multi-resolution maps ($B=4$); we compute $y^{(i)} = \mathcal{A}^{(i)}(f^{(i)})$, $\mathcal{A}^{(i)} \in \{\text{SE BLOCK, CBAM}\}$. Because gating is multiplicative and zero-initialized, tensor shapes and channels are unchanged, so the YOLC neck/head need no code changes.

4. EXPERIMENTS AND RESULTS

4.1. Datasets

Modified DOTA v2.0. Given the focus of this research on enhancing the detection of tiny objects, a dataset tailored to such targets was essential. To this end, we modified the original DOTA 2.0 dataset by selectively retaining only those object categories that consistently exhibit small spatial footprints in aerial imagery. The resulting modified dataset comprises five classes: *small vehicle*, *large vehicle*, *ship*, *plane*, and *storage tank*. Since the modified dataset was used, the evaluation could not be done through evaluation server but was performed locally using the test set. The dataset is in the repository.

Table 1: Object categories of the Modified-DOTA



Table 2: Dataset Size Comparison

Dataset	Average pixel size
Aerial Imagery Dataset	
UCAS-AOD [17]	$\approx 4149 \text{ px}^2$ (64.4×64.4)
VisDrone [18]	$\approx 2490 \text{ px}^2$ (49.9×49.9)
DOTAv2.0 [19]	$\approx 3394 \text{ px}^2$ (58.2×58.2)
Modified-DOTA (Ours)	$\approx \mathbf{968 \text{ px}^2}$ ($\mathbf{31.1 \times 31.1}$)
Small Object Category Threshold	
COCO -"small" [20]	1024 px^2 (32×32)
Modified-DOTA (Ours)	$\approx \mathbf{968 \text{ px}^2}$ ($\mathbf{31.1 \times 31.1}$)

As it can be seen in the table 2, the retained objects in our modified dataset occupies approximately **968 pixels²** corresponding roughly to a **31×31 pixel bounding region**. This area is below widely accepted thresholds for small objects, such as the 1024 pixels² cutoff defined in the COCO dataset for "small" instances [20].

VisDrone. We also evaluated on the VisDrone benchmark to assess generalization and enable fair comparison. Table 5 reports backbone ablations (identifying the best backbone), and Table 8 benchmarks our approach against state-of-the-art methods in tiny-object detection. Since the VisDrone server is currently unavailable, we used the validation set for evaluation.

4.2. Training Setting

All training was conducted in a secure cloud using one NVIDIA L40S GPU, 32 vCPUs, and 125 GB RAM. The environment ran PyTorch 2.2.0, Python 3.10, and CUDA 12.1.1 on Ubuntu 22.04.

Trial Screening: Input image adjustment, augmentation, and backbone testing were performed over 50 epochs (batch size 4, 640×640 image size) using the SGD optimizer and a modified, non-augmented DOTA dataset. The trainings used pretrained YOLOv8n.

Final Training: The YOLOv8n with the default and MoonNet backbones were trained for 150 epochs with batch size 4 and the selected candidates setting. The YOLC model trainings were conducted for 50 epochs.

Evaluation Metrics: Performance was evaluated using AP_{50} , AP , recall, and precision for YOLOv8; and AP_{50} , AP_{75} , and AP for YOLC in MMDetection. AP_{50} and AP_{75} are obtained at the single IoU threshold 0.5 and 0.75 over all categories. AP is obtained by averaging over threshold 0.5 to 0.95 over all categories.

4.3. Input image resolution adjustment

Identified 928 as yielding the highest performance.

Table 3: Performance comparison across image size

Input image resolution	AP_{50}	AP	Recall	Precision
(640×640)	0.323	0.180	0.279	0.638
(800×800)	0.344	0.199	0.301	0.741
(928×928) ✓	0.372	0.208	0.331	0.635

4.4. Data Augmentation

A total three of different augmentation packages were tested and the implemented augmentation types were explained in table 4. **Geo**-denotes geometric transformations, **BBox**-denotes bounding box transformation, and **Color/Blur**-denotes noise and color adjustment.

Table 4: Performance metrics across augmentation

Package	Geo	BBox	Color/Blur	AP_{50}	AP	Recall	Precision
Ver 1				0.323	0.180	0.279	0.638
Ver 2 ✓	✓			0.371	0.213	0.325	0.662
Ver 3	✓	✓	✓	0.344	0.194	0.303	0.648

4.5. Attention Mechanism

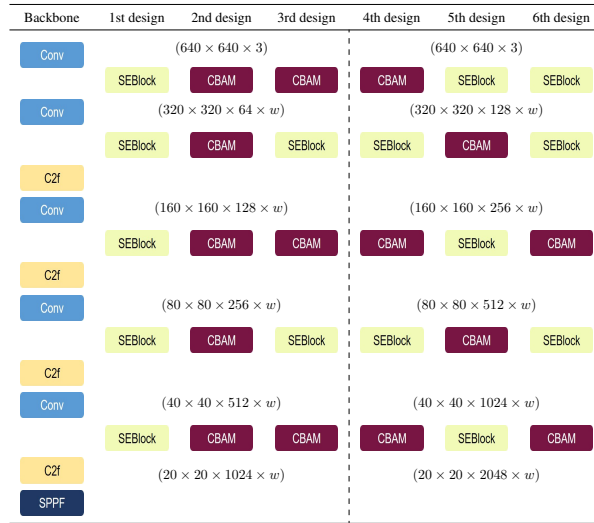
Total six attention-augmented backbones were tested in table 5 and the backbone designs are displayed in table 6. The two modules were attached to the CNN layers of the original YOLO backbone in different arrangements.

MoonNet: The fifth design obtained the best performance among the backbone designs. We name this particular backbone with SE Block-CBAM arrangement as **Mixture of Orthogonal Neural-modules Network(MoonNet)** and this backbone is used for the final training adapted to the YOLOv8 and YOLC model.

Table 5: Backbone results

Augmented Backbone	AP_{50}	AP	Recall	Precision
Dataset: Modified DOTAv2.0 (50 epochs)				
Default	0.286	0.142	0.262	0.547
1st Design	0.289	0.143	0.271	0.527
2nd Design	0.283	0.142	0.264	0.503
3rd Design	0.274	0.131	0.258	0.577
4th Design	0.336	0.177	0.301	0.625
5th Design ✓	0.344	0.180	0.301	0.687
6th Design	0.342	0.178	0.315	0.593
Dataset: VisDrone (150 epochs)				
5th Design ✓	0.360	0.216	0.347	0.467
6th Design	0.358	0.214	0.352	0.453

Table 6: Backbone designs



4.6. Final training and ablation studies

The final MoonNet-based model was trained from scratch with optimized input image resolutions and augmentations, showing clear improvements over the default YOLOv8n. In Table 7, **Default** refers to the original backbone, **Res** to optimized input image resolution, and **Aug** to optimized augmentations. The number of channels from the model’s backbone in the final training is not identical to the numbers presented in table 5. This is because all the final trainings in the table 7 were conducted using YOLOv8n model scale thus actual number of channels were (32, 64, 128, 256, 512) due to the channel multiplier (0.25). For the fair comparison, all the backbones in table 7 used same number of channels.

Table 7: Performance metrics for final models

Method	Default	MoonNet	Res	Aug	AP_{50}	AP	Recall	Precision
Method 1	✓				0.397	0.236	0.356	0.638
Method 2	✓		✓		0.439	0.268	0.387	0.680
Method 3	✓		✓	✓	0.441	0.268	0.375	0.766
Method 4		✓	✓	✓	0.504	0.299	0.442	0.781

Image resolution adjustment (Method1 → Method2)

Varying the input image resolution yields +10.58% gain in AP_{50} and +13.56% gain in AP showing improved optimization helps recover missed tiny objects.

Proper data augmentation (Method2 → Method3)

Adding geometric transformations such as rotation and flip steadies generalisation: AP_{50} rises slightly to 0.441, while AP stays the same.

Effectiveness of MoonNet (Method3 → Method4)

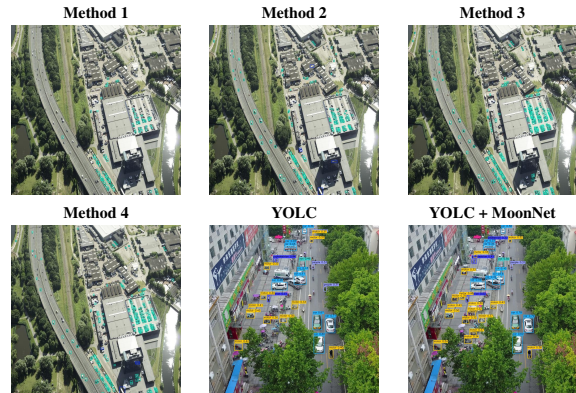
Replacing the vanilla CSP with MoonNet achieves the highest scores: 0.504 AP_{50} and 0.299 AP . This yields +14.29% gain and +11.57% gain over the tuned backbone, and +26.91% gain in AP_{50} over the baseline.

Table 8: The state-of-the-art comparison on VisDrone

Method	Backbone	AP	AP_{50}	AP_{75}
ClusDet[21]	ResNet101	0.267	0.504	0.252
ClusDet[21]	ResNeXt101	0.284	0.532	0.264
DMNet [22]	ResNet101	0.285	0.481	0.294
DMNet [22]	ResNext101	0.294	0.493	0.306
YOLC(k=1) [12]	HRNet	0.303	0.516	0.307
YOLC(k=1) [12]	HRNet + MoonNet(Ours)	0.329	0.550	0.336

In table 8, the MoonNet’s attention module arrangement was integrated into the YOLC model and achieved state-of-the-art performance when compared with ClusDet[21] and DMNet[22], both trained on cluster-aware cropped images. Ours obtained +15.87% gain compared to ClusDet, +11.9% gain compared to DMNet and +8.58% gain against the original YOLC.

Table 9: Visual comparison



5. CONCLUSION

This research improves tiny object detection by combining resolution adjustment, augmentation, and the MoonNet backbone. Compared to default YOLOv8, the final model (Model 4) achieved gains of +26.96% AP_{50} , +26.69% AP , +24.16% recall, and +22.41% precision. In addition, the MoonNet integrated backbone achieved state-of-the-art performance among the cluster-aware detectors confirming attention-augmented backbone enhances detection of small targets in aerial imagery.

6. REFERENCES

- [1] Ross Girshick, Jeff Donahue, Trevor Darrell, and Jitendra Malik, “Rich feature hierarchies for accurate object detection and semantic segmentation,” in *CVPR*, 2014, pp. 580–587.
- [2] Shaoqing Ren, Kaiming He, Ross Girshick, and Jian Sun, “Faster R-CNN: Towards real-time object detection with region proposal networks,” in *NeurIPS*, 2015, pp. 91–99.
- [3] Tsung-Yi Lin, Piotr Dollár, Ross Girshick, Kaiming He, Bharath Hariharan, and Serge Belongie, “Feature pyramid networks for object detection,” in *CVPR*, 2017, pp. 2117–2125.
- [4] Kaiming He, Georgia Gkioxari, Piotr Dollár, and Ross Girshick, “Mask R-CNN,” in *ICCV*, 2017, pp. 2961–2969.
- [5] Wei Liu, Dragomir Anguelov, Dumitru Erhan, Christian Szegedy, Scott Reed, Cheng-Yang Fu, and Alexander C. Berg, “SSD: Single shot multi-box detector,” in *ECCV*, 2016, pp. 21–37.
- [6] Joseph Redmon, Santosh Divvala, Ross Girshick, and Ali Farhadi, “You only look once: Unified, real-time object detection,” 2016, vol. 2016-December.
- [7] Joseph Redmon and Ali Farhadi, “YOLOv3: An incremental improvement,” in *arXiv preprint arXiv:1804.02767*, 2018.
- [8] Mingyang Ma and Huanli Pang, “Sp-yolov8s: An improved yolov8s model for remote sensing image tiny object detection,” *Applied Sciences*, vol. 13, no. 14, pp. 8161, 2023.
- [9] Mengzi Hu, Ziyang Li, Jiong Yu, Xueqiang Wan, Haotian Tan, and Zeyu Lin, “Efficient-lightweight yolo: Improving small object detection in yolo for aerial images,” *Sensors*, vol. 23, no. 14, pp. 6423, 2023.
- [10] Chang Xu, Jinwang Wang, Wen Yang, Huai Yu, Lei Yu, and Gui-Song Xia, “Detecting tiny objects in aerial images: A normalized wasserstein distance and a new benchmark,” *ISPRS Journal of Photogrammetry and Remote Sensing*, vol. 190, pp. 79–93, 2022.
- [11] Chenhongyi Yang, Zehao Huang, and Naiyan Wang, “Querydet: Cascaded sparse query for accelerating high-resolution small object detection,” in *CVPR*, 2022, pp. 13658–13667.
- [12] Wei Chen, Sui Yang, Jie Xu, and Jun Li, “Yolc: Yolo with clusters for improved object detection,” in *CVPR*. IEEE, 2021, pp. 10201–10210.
- [13] Longbin Yan, Yunxiao Qin, and Jie Chen, “Scale-balanced real-time object detection with varying input-image resolution,” *IEEE Transactions on Circuits and Systems for Video Technology*, vol. 33, pp. 242–256, 1 2023.
- [14] Mate Kisantal, Zbigniew Wojna, Jakub Murawski, Jacek Naruniec, and Kyunghyun Cho, “Augmentation for small object detection,” 2019.
- [15] Jie Hu, Li Shen, Samuel Albanie, Gang Sun, and Enhua Wu, “Squeeze-and-excitation networks,” *IEEE Transactions on Pattern Analysis and Machine Intelligence*, vol. 42, 2020.
- [16] Sanghyun Woo, Jongchan Park, Joon Young Lee, and In So Kweon, “Cbam: Convolutional block attention module,” 2018, vol. 11211 LNCS.
- [17] Haigang Zhu, Xiaogang Chen, Weiqun Dai, Kui Fu, Qixiang Ye, and Jian Jiao, “Orientation robust object detection in aerial images using deep convolutional neural network,” in *ICIP*, 2015, pp. 3735–3739.
- [18] Pengfei Zhu, Longyin Wen, Dawei Du, Xiao Bian, Heng Fan, Qinghua Hu, and Haibin Ling, “Detection and tracking meet drones challenge,” *IEEE Transactions on Pattern Analysis and Machine Intelligence*, vol. 44, no. 11, pp. 7380–7399, 2021.
- [19] Gui-Song Xia, Xiang Bai, Jian Ding, Zhen Zhu, Serge Belongie, Jiebo Luo, Mihai Datcu, Marcello Pelillo, and Liangpei Zhang, “Dota: A large-scale dataset for object detection in aerial images,” in *CVPR*, 6 2018.
- [20] Tsung-Yi Lin, Michael Maire, Serge Belongie, James Hays, Pietro Perona, Deva Ramanan, Piotr Dollár, and C. Lawrence Zitnick, “Microsoft COCO: Common objects in context,” in *ECCV*. 2014, pp. 740–755, Springer.
- [21] Fan Yang, Heng Fan, Peng Chu, Erik Blasch, and Haibin Ling, “Clustered object detection in aerial images,” in *ICCV*, October 2019, pp. 8310–8319.
- [22] Changlin Li, Taojiannan Yang, Sijie Zhu, Chen Chen, and Shanyue Guan, “Density map guided object detection in aerial images,” in *CVPRW*, 2020, pp. 737–746.